Journal of Molecular Graphics and Modelling 27 (2008) 529–535

Contents lists available at ScienceDirect

Journal of Molecular Graphics and Modelling

journal homepage: www.elsevier.com/locate/JMGM

Insights into thermal stability of thermophilic nitrile hydratases by molecular dynamics simulation

Jie Liu, Huimin Yu *, Zhongyao Shen

Department of Chemical Engineering, Tsinghua University, Beijing 100084, China

ARTICLE INFO

Article history:
Received 21 May 2008
Received in revised form 28 August 2008
Accepted 2 September 2008
Available online 10 September 2008

Keywords:
Thermal stability
Thermophilic nitrile hydratase
Molecular dynamic simulation
Root mean square fluctuation
Salt-bridge interaction

ABSTRACT

Thermal stability is of great importance for industrial enzymes. Here we explored the thermal-stable mechanism of thermophilic nitrile hydratases (NHases) utilizing a molecular dynamic simulation. At a nanosecond timescale, profiles of root mean square fluctuation (RMSF) of two thermophilic NHases, 1UGQ and 1V29, under enhancing thermal stress were carried out at 300 K, 320 K, 350 K and 370 K, respectively. Results showed that the region A1 (211–231 aa) and A2 (305–316 aa) in 1UGQ, region B1 (186–192 aa) in 1V29, and most of terminal ends in both enzymes are hyper-sensitive. Salt-bridge analyses revealed that in one hand, salt-bridges contributed to maintaining the rigid structure and stable performance of the thermophilic 1UGQ and 1V29; in the other hand, salt-bridges involved in thermal sensitive regions are relatively weak and prone to be broken at elevated temperature, thereby cannot hold the stable conformation of the spatial neighborhood. In 1V29, region A1 was stabilized by a well-organized hook–hook like cluster with multiple salt-bridge interactions, region A2 was stabilized by two strong salt-bridge interactions of GLU52-ARG332 and GLU334-ARG332. In 1UGQ, the absence of a charged residue decreased its thermal sensitivity of region B1, and the formation of a small β-sheet containing a stable salt-bridge in C-β-terminal significantly enhanced its thermal stability. By radius of gyration calculation containing or eliminating the thermal sensitive regions, we quantified the contribution of thermal sensitive regions for thermal sensitivity of 1UGQ and 1V29. Consequently, we presented strategies to improve thermal stability of the industrialized mesophilic NHase by introducing stable salt-bridge interactions into its thermal sensitive regions.

1. Introduction

Thermal stability of enzymes has attracted great attention recently since the fast development of the industrial biocatalysis. For example, the nitrile hydratase (NHase), which catalyzes the bioconversion of nitriles to corresponding amides in several microorganisms, is currently widely used in the industrial production of high purity acrylamide [1]. However, most of the industrialized NHases with high activity are remarkably unstable. For instance, the NHases of *Rhodococcus* sp. N-774 and *P. chlororaphils* B23 are merely stable under 20 °C [2,3], and the NHase of *Rhodococcus rhodochrous* J1 is merely stable between 10 and 30 °C [4]. Since the nitrile-hydration is an exothermic reaction, the industry has to maintain this low reaction temperature to stabilize the NHases by refrigeration, which usually causes tremendous unwanted energy cost. As thermophilic enzymes usually exhibit a promising potential for biotechnological applications where generally require ambient or higher temperature for a catalysis process, it is of great importance to figure out which key factors governing the thermal stability of proteins, provide essential rational approaches for supporting the adaptation of the regular mesophilic enzymes.

Generally, thermal stability of a thermophilic enzyme is associated with the free energy difference between the native and denatured state. For different enzymes, the contribution arises from different factors, including the introduction of additional disulfide bridges, improvement in the compactness of the hydrophobic core, intensification of surface salt-bridge networks or alpha-helix dipole interactions to enhance the enthalpy contribution, and substitution of X-to-Pro and Gly-to-Ala to enhance the entropy contribution [5]. Basically, the thermal stability improvement usually requires a combination of multiple amino acid exchanges, consequently increases the melting temperature of the enzyme. To date, the most effective rational

* Corresponding author. Tel.: +86 10 62788568; fax: +86 10 62770304.
E-mail address: yuhm@tsinghua.edu.cn (H. Yu).

1093-3263/$ – see front matter © 2008 Elsevier Inc. All rights reserved.
doi:10.1016/j.jmgm.2008.09.004

way to evaluate these factors is molecular dynamics (MD) simulation, which can utilize the microscopic information such as atomic coordinates, velocities and energies associated with the thermal enhancing factors [6]. This approach has been widely used in the investigation of a wide range of dynamic properties and progresses in numerous fields. For instance, using the MD simulation, the thermal stable mechanism of Rubredoxin [7], *Staphylococcal* nuclease [8], barnase [9], and adenylate kinase have been observed [10].

In this study, MD simulations were carried out for two moderate thermophilic NHases from different sources to explore the key factors governing the thermal stability of NHases. By calculating the root mean square deviation (RMSD) and root mean square fluctuation (RMSF) values for backbone atoms, thermal sensitive regions of both NHases were identified. The thermal-response behavior and salt-bridge interactions in these regions were analyzed and the thermal stable mechanism of thermophilic NHases was presented.

2. Methodology

2.1. Simulation set up and configuration

The crystal structures used in the MD simulation were obtained from the Protein Data Bank (PDB) database with PDB code of 1UGQ [11,12] and 1V29 [13], originally isolated from the *Pseudonocardia thermophila* JCM3095 [14] and thermophilic *Bacillus* SC-105-1 [13], respectively. The MD simulations were carried out by Amber 8.0 software with a Parm99 force filed [15]. Hydrogen atoms were added by the 'tleap' facility, and Na^+ was also added to neutralize the system. The pH 7.0 was set as default. Proteins were solvated in a cubic box consisting TIP3P water molecules and the box size was chosen by the criterion that the distance of protein atoms from the wall was greater than 10.0 Å. An Ewald summation method was used for calculating the total electrostatic energy in a periodic box named Particle Mesh Ewald (PME) [16]. The other non-bonded interactions were calculated by L-J model with a cutoff distance of 10 Å.

Structure minimization was performed to remove any unexpected coordinate collision and get the local minima. The water box and the whole system were minimized using the descent method (1000-step and 2000-step, respectively) plus the conjugate gradient method. The overall RMSD of the minimized 1UGQ and 1V29 from their crystal structures is 0.6742 Å and 0.5479 Å, respectively, indicating that the Parm99 force field is suitable for simulations. RMSF of 1UGQ and 1V29 from the MD trajectories at 300 K was also calculated and compared with the crystallographic B-factor [17], another indicator of the backbone flexibility, consequently a global consistency was achieved which confirming that the MD simulation in this system is reliable.

2.2. System heating, equilibration and data sampling

After minimization, the system heating, equilibration and data sampling were carried out in turn. The system heating was performed gradually from 0 K to the desired temperature in a NTV ensemble, followed by a further 150 ps simulation for equilibration and 1 ns or longer simulation for data sampling in a NTP ensemble. The temperature was set as 300 K, 320 K, 350 K and 370 K, respectively, at 1 atm pressure. Weak-coupling algorithm was used for the temperature and pressure regulation with a coupling time of 1.0 ps. SHAKE method was used for constraining the bonds with hydrogen.

3. Results and discussion

3.1. Identification of thermal sensitive regions by global RMSF search under thermal stress

Average RMSF values in the MD simulation were usually considered as the criterion for overall flexibility of the system. By MD simulations at multiple temperatures, RMSFs of backbone atoms against each residue were calculated over the last 800 ps for both enzymes. As shown in Fig. 1a and b, RMSFs in most regions of 1UGQ and 1V29 merely showed slight fluctuations with the increase of temperature, indicating that these regions are relatively thermal-stable. On the contrary, some specific regions exhibited steep RMSF-fluctuations at elevated temperature such as 350 K or 370 K, indicating that these are the thermal hyper-sensitive regions.

For 1UGQ in Fig. 1a, these thermal hyper-sensitive regions such as A1 (211–231 aa) and A2 (305–316 aa), mainly located in the β-subunit which stands in the latter-part of the *X*-axis with amino acid sequence of 204–431 aa. Terminals of N-α- and N-β-subunit also exhibited a significant sensitivity to thermal stress, but the C-β-terminal was considerably stable. For 1V29 in Fig. 1b, it can be seen that a new sensitive region of B1 (186–192 aa) occurred in the α-subunit, and all terminals including N-α-, C-α-, N-β- and C-β-subunit showed hyper thermal sensitivity. Fig. 1c illustrated the RMSF comparison between 1UGQ and 1V29 specifically at 350 K. It was interestingly found that the hyper-sensitive regions A1 and A2 in 1UGQ were obviously stabilized in 1V29, meanwhile the sensitive regions of B1 and C-β-terminal in 1V29 were stabilized in 1UGQ.

3.2. Conformation changes of thermal sensitive regions

To further clarify the trait of the thermal sensitive structure, conformation changes of 1UGQ at $t = 893$ ps from $t = 0$ ps were calculated and illustrated in Fig. 2. Thermal sensitive regions including N-α-terminal, N-β-terminal, A1 and A2 were labeled. It can be seen that all of these thermal sensitive regions are coils or loops located in the surface of 1UGQ, and the conformation at $t = 893$ ps obviously deviated from the original position at $t = 0$ ps. According to previous studies on protein unfolding under thermal stress, these large fluctuations of surface loops and terminals would trigger an unfolding process and consequently denature the 1UGQ. Similar results were also obtained for 1V29.

3.3. Profile of salt-bridge interactions

Previous studies have suggested that the dominant factor determining thermal stability of thermophilic and mesophilic NHases would be intramolecular interactions [19]. These interactions, served as enthalpy contribution to thermal stability, mainly include hydrophobic interactions, hydrogen bonds or salt-bridges. Many MD studies have shown that in the native state, these interactions may become weaker or even absent as temperature increases [20]. Among these interactions, salt-bridges play important roles in contribution to the folding free energy of thermophilic proteins, therefore becoming our major focus to uncover the stabilizing mechanism of 1UGQ and 1V29.

Using the hydrogen bonding facility of Amber 8.0 [15], we calculated salt-bridge interactions between positive and negative charged residues throughout amino acid residues of 1UGQ and 1V29 under enhancing thermal press, and summarized results in the lower-layer of Fig. 1 by cross mark labeling. As can be seen, both 1UGQ and 1V29 possess a great number of stable salt-bridges. This is reasonable because both of them belong to thermophilic

enzymes. These salt-bridges serve as multiple separate spikes to hold the conformation against thermal stress. However, most salt-bridges are weakened or even completely disappeared at elevated thermal stress in the thermal sensitive regions, due to the kinetic energy improvement of atoms involved in the hydrogen bond, accordingly inducing the conformation deviation from regular positions. For example, the salt-bridge GLU^{268}-ARG^{6} in the N-α-terminal of 1UGQ was weakened at first at 350 K with merely 68% occupied time, then completely disappeared at 370 K.

3.4. Salt-bridge interaction comparison in region A1 and A2 of 1UGQ and 1V29

To further explore the stabilization mechanism of region A1 and A2 in 1V29, side-chain salt-bridge profiles in both 1UGQ and 1V29 were calculated and compared in Table 1. Simultaneously, the amino acid sequences of both regions were listed in Fig. 3a (region A1) and Fig. 3b (region A2), respectively.

As can be seen, in region A1 of 1UGQ (residue 211–231 aa), there are two ARG (ARG^{221} and ARG^{229}), two ASP (ASP^{214} and ASP^{224}) and two GLU (GLU^{225} and GLU^{231}) residues, respectively (Fig. 3a), in which GLU^{145}-ARG^{221} form a salt-bridge with an average distance of 2.9 Å at 300 K. This salt-bridge provides a moderate stable spike holding the conformation of A1. However, the occupied time of simulation for this salt-bridge reduced to 55% at 350 K, indicating that this interaction became weaken as the temperature enhances. Additionally, residue ARG^{229} simultaneously encountered static affinities from three carboxyl groups in residues of GLU^{225}, GLU^{127} and GLU^{233} (as shown in Fig. 4), which caused unstable and alterable interactions within these residues. For example, the closest distance within side-chain O–N atoms changed from 4.67 Å in GLU^{225}-ARG^{229} at $t = 0$ ps to 4.30 Å in GLU^{233}-ARG^{229} at $t = 540$ ps. As a result, the salt-bridge interaction of GLU^{225}-ARG^{229} at 300 K disappeared at 320 K, but forming a new salt-bridge interaction by ARG^{229} re-bending towards GLU^{233}. Collectively, salt-bridges within the thermal sensitive region A1 of 1UGQ are not adequately strong to "spike" their adjacent structures from dissolving into solvent, thereby cannot stably maintain the rigid 3D structure under enhanced thermal stress.

Additionally, most of negative charged residues in region A1 of 1UGQ are not included in any couples of salt-bridges. These

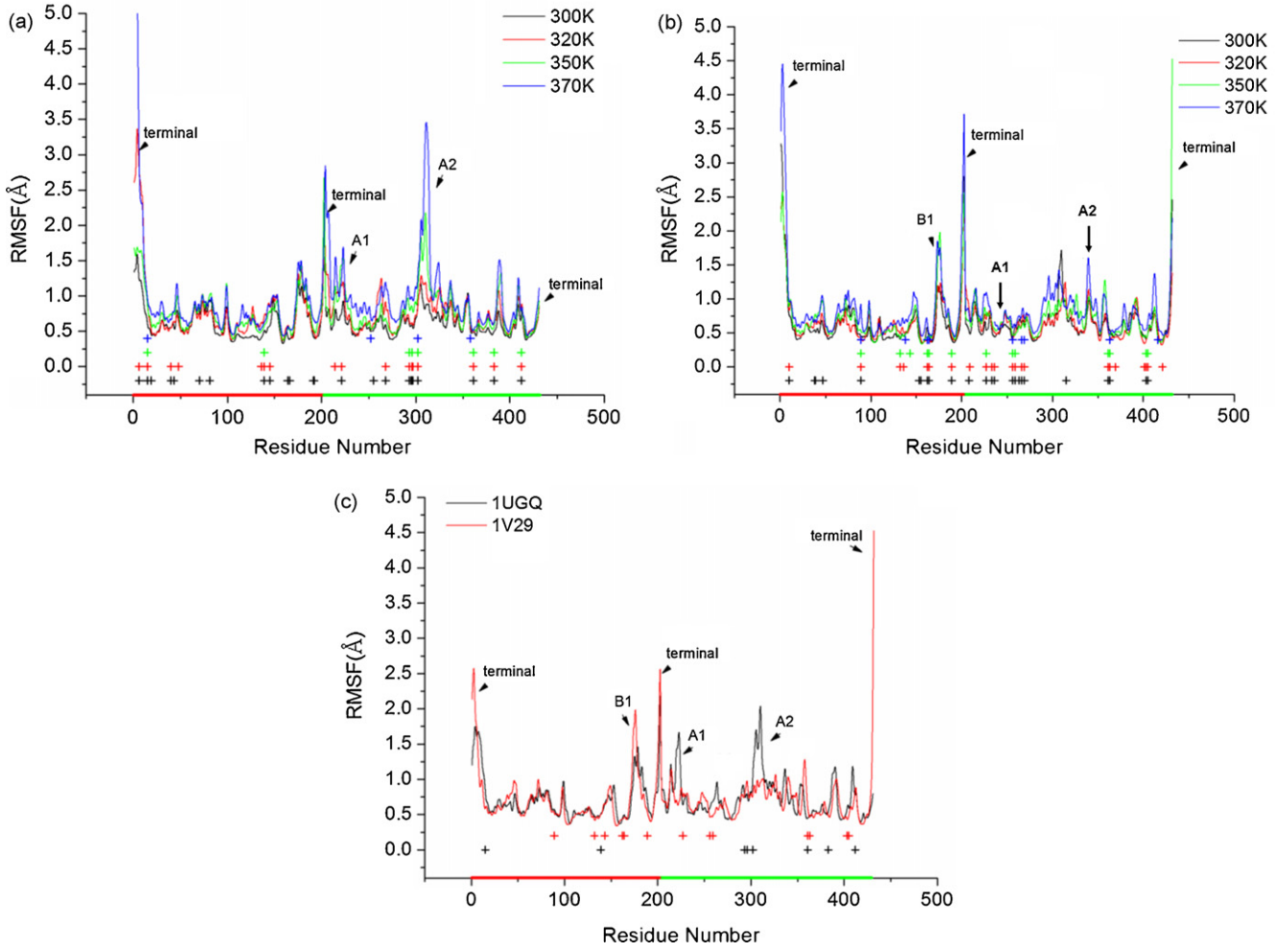

Fig. 1. Global fluctuations of 1UGQ and 1V29 under enhancing thermal stress. The red segment along the *X*-axis indicates the α-subunit while the green segment corresponds to the β-subunit. The cross marker along the *X*-axis represents a charged residue forming a stable salt-bridge during the simulation (longer than 80% occupied time with a distance less than 3 Å) at 300 K (black), 320 K (red), 350 K (green) and 370 K (blue), respectively. (a) RMSFs against residues for 1UGQ at 300 K (black), 320 K (red), 350 K (green) and 370 K (blue). Thermal sensitive regions of A1, A2 and respective terminals of α- and β-subunit were indicated by arrows. (b) RMSFs against residues for 1V29 at 300 K (black), 320 K (red), 350 K (green) and 370 K (blue). Arrows indicated thermal-sensitive regions of B1 and all terminals in 1V29, and corresponding regions of A1 and A2 in 1UGQ, respectively. (c) RMSF-superposition of 1UGQ and 1V29 at 350 K. Thermal sensitive terminals and region A1, A2 and B1 are marked by arrows, respectively. Black, 1UGQ; red, 1V29.

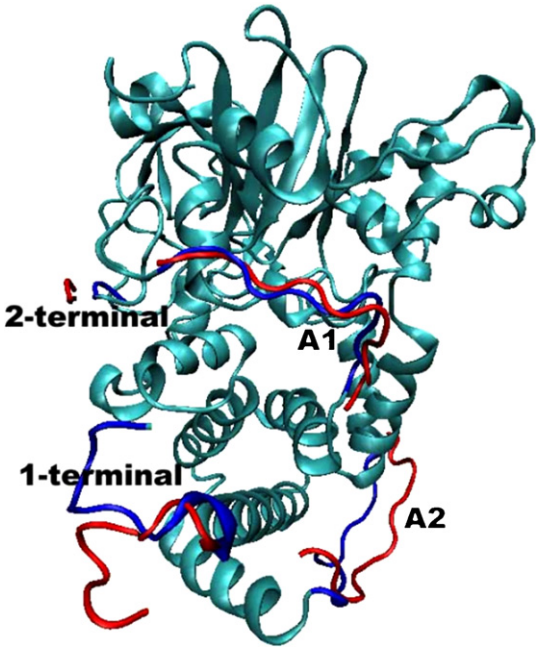

Fig. 2. Tertiary structure of 1UGQ illustrating conformation changes of thermal sensitive regions of A1, A2, and terminals plotted by the software VMD [18]. The blue color in thermal sensitive regions represents the original conformation at 370 K, while the red color represents the simulated conformation at t = 893 ps at 370 K. 1-termial and 2-terminal represent the N-α- and N-β-terminal, respectively.

a. A1 region

1UGQ	211	GGTDGLGPINRP--ADEPVFRAE	231
1V29	228	GGMDGFGKIMYVKEEEDTYFKHD	250
AY168347	211	GGMTGYGPVPYQ--KDEPFFHYE	231

b. A2 region

1UGQ	305	PDAPLPEHEQKP	316
1V29	326	PDTKIQRWEN-P	336
AY168347	308	RYTDRNPSRKFD	319

c. B1 region

1UGQ	174	PAGTDGW	180
1V29	186	PEGTEGM	192
AY168347	168	PAGTDGW	175

d. C-β-terminal

1UGQ	426	IELVDT	431
1V29	444	LEPVSH	449
AY168347	429	LISA--	432

Fig. 3. Protein sequence alignment of 1UGQ, 1V29 and AY168347. a, b, c, and d, amino acid alignment in thermal sensitive regions of A1 and A2 in 1UGQ, B1 and C-β-terminal in 1V29, respectively.

residues would favorably interact with water and expose their adjacent hydrophobic core directly into the solvent, consequently resulting into the 1UGQ denaturation.

In region A1 of 1V29 (residues of 228–250 aa), there are several charged residues including ASP^{231}, LYS^{235}, LYS^{240}, GLU^{241}, GLU^{242}, GLU^{243}, ASP^{244} and LYS^{248}, as shown in Fig. 3a. Unlike the dispersed distribution of the charged residues in 1UGQ, residues LYS^{240}, GLU^{241}, GLU^{242}, GLU^{243} and ASP^{244} in 1V29 form a short α-helix (Helix A1) with an axis towards inside. This short helix itself works as a stable hook in one hand, simultaneously hanging A1 to another short α-helix named "Helix B" (ARG^{203}-ASP^{204}-SER^{205}-MET^{206}-ILE^{207}-GLU^{208}-VAL^{209}) in the other hand, where Helix B is close to the hydrophobic core. As illustrated in Fig. 5, we can see that this hook–hook like structure fits with each other perfectly by stable hydrogen bond interactions of GLU^{241}-ARG^{203}, ASP^{204}-GLU^{241} and ASP^{244}-ARG^{203}, preventing the bending motion of A1 occurred in 1UGQ. Here the salt-bridge in ASP^{244}-ARG^{203} is a side-chain/side-chain interaction which was maintained stable at 350 K, as listed in Table 1, but the salt-bridge interactions in GLU^{241}-ARG^{203} were generated within two side chain oxygen atoms in GLU^{241} (hydrogen bonding donor) and one main chain nitrogen atom in ARG^{203} (hydrogen bonding acceptor). The strong hydrogen bonds within ASP^{204}-GLU^{241} were also formed by two side-chain oxygen atoms in ASP^{204} and one main-chain nitrogen atom in GLU^{241}. Interaction changes of these side-chain/main-chain salt-bridges under thermal stress were summarized in Table 2. We can see that the GLU^{241}-ARG^{203} interactions remained stable even at 370 K. Collectively, the hook–hook like structure held by these multiple salt-bridge interactions in region A1 of 1V29 significantly decreased its flexibility.

In region A2 of 1UGQ (residues of 305–316 aa), there's no salt-bridge interaction observed within the four charged residues:

Table 1
Salt-bridge interactions within thermal sensitive regions of A1 and A2[a].

Amino acids		Occupied time (%)	Distance (Å)	Angle (°)	Amino acids		Occupied time (%)	Distance (Å)	Angle (°)
1UGQ 300 K					1V29 300 K				
GLU^{145}	ARG^{221}	99	2.942	22.69	ASP^{244}	ARG^{203}	100	2.786	16.61
GLU^{225}	ARG^{229}	74	3.426	32.28	GLU^{52}	ARG^{332}	100	2.891	19.39
ASP^{214}	ARG^{136}	52	3.263	41.23	GLU^{334}	ARG^{332}	98	3.239	29.08
1UGQ 320 K					1V29 320 K				
ASP^{214}	ARG^{136}	96	2.946	26.75	ASP^{244}	ARG^{203}	100	2.791	19.71
GLU^{145}	ARG^{221}	95	3.028	24.66	GLU^{334}	ARG^{332}	97	3.534	28.10
GLU^{233}	ARG^{229}	73	3.294	36.97	GLU^{52}	ARG^{332}	91	3.229	29.11
1UGQ 350 K					1V29 350 K				
GLU^{233}	ARG^{229}	64	4.000	32.95	ASP^{244}	ARG^{203}	100	2.808	20.65
GLU^{145}	ARG^{221}	55	3.574	31.13	GLU^{52}	ARG^{332}	97	3.126	27.21
					GLU^{334}	ARG^{332}	95	3.623	26.66
1UGQ 370 K					1V29 370 K				
GLU^{233}	ARG^{229}	90	3.559	26.42	GLU^{52}	ARG^{332}	96	3.192	33.72
GLU^{145}	ARG^{221}	55	2.994	26.49	GLU^{334}	ARG^{332}	96	3.409	28.88

[a] The criteria for determining salt-bridges are: carboxyl oxygen atoms on the side-chain of ASP, GLU are hydrogen bonding donors; hydrogen and nitrogen atoms connected together on the side-chain of LYS, ARG or GLU are hydrogen bonding acceptors. Time occupancy cutoff during the simulation is 50%. Distance cutoff is 5.00 angstroms (Å), and O–H–N angle cutoff is 120.00°. Intra-residue interactions were not included. Data were sorted by the value of the occupied time.

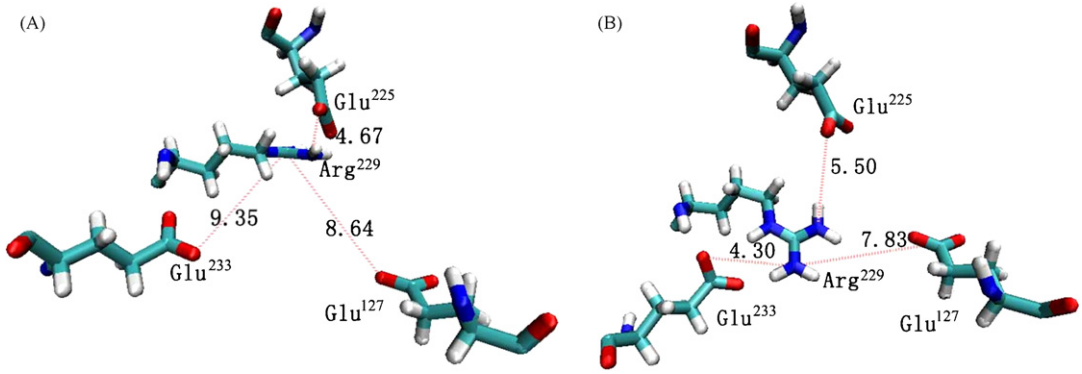

Fig. 4. Conformation sketch map of region A1 in 1UGQ involving charged residues of ARG^{229}, GLU^{225}, GLU^{127} and GLU^{233}. (A) t = 0 ps, T = 300 K. (B) t = 540 ps T = 300 K. The dashed line represents a hydrogen bonding interaction with distance pointed out by the adjacent number. Red, oxygen atom; blue, nitrogen atom; cyan, carbon atom; white, hydrogen atom.

ASP^{306}, GLU^{311}, GLU^{313} and LYS^{315} (Fig. 3b). These residues are prone to interact with water solvent, consequently enlarging the fluctuation of this region. However, in the corresponding domain of 1V29 (residues 326–336 aa, Fig. 3b), two salt-bridges, GLU^{52}-ARG^{332} and GLU^{334}-ARG^{332}, are formed with quite stable interactions at all observed temperatures, as shown in Table 1, which would explain the remarkable stabilization of the A2 region in 1V29.

3.5. Structure analyses of region B1 and C-β-terminal in 1UGQ and 1V29

In region B1 (Fig. 3c), no stable interaction was found for both 1UGQ and 1V29, in agreement with their relative large RMSFs. In comparison to 1UGQ, the B1 region in 1V29 (186–192 aa) contains an extra charged residue of GLU^{187}, probably being responsible for its much higher fluctuation.

Additionally, the C-terminal end of the β-subunit in 1UGQ (residues 426–431 aa, Fig. 3d) forms a small β-sheet containing a stable salt-bridge (THR^{431}-LYS^{343}) at an average distance of 3 Å, therefore remaining quite stable even at 370 K as shown in Fig. 1a. While in 1V29, this region is merely a regular loop structure (residues 444–449 aa, Fig. 3d) without any salt-bridge interaction, consequently causing a large fluctuation under elevated thermal stress (Fig. 1b).

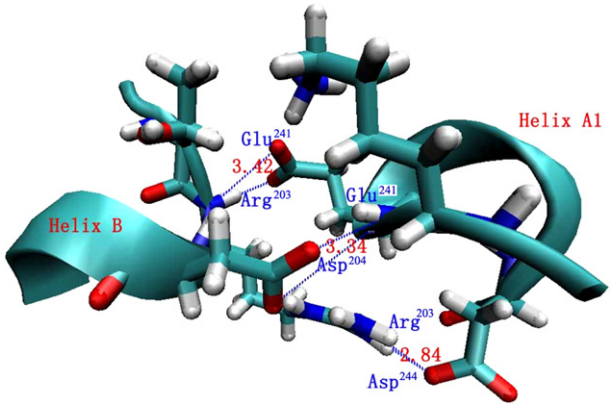

Fig. 5. Conformation sketch map of the hook–hook like structure in region A1 of 1V29. Helix A1 binds Helix B closely with stable salt-bridge interactions. The image arises from a mean conformation at 300 K. Red, oxygen atom; blue, nitrogen atom; cyan, carbon atom; white, hydrogen atom. Dashed lines indicate hydrogen bonding interactions and numbers describe the mean hydrogen bond distance.

3.6. Quantifying RMSF contributions of the major thermal sensitive regions

To get a global review of the heating denaturation mainly caused by the thermosensitive regions, radiuses of gyration (R_g) of 1UGQ (Fig. 6A) and 1V29 (Fig. 6B) were calculated with the conformations from the trajectories at a time interval of 10 ps using MMTSB scripts [21]. We can see that the radius is vibrated around 22.2 Å below 350 K for either 1UGQ or 1V29, like a normal "breathing" activity. This kind of mild breathing becomes wild when the temperature increases to 370 K, suggesting that some regions have lost their native compactness and dissolved into the solvent as a result of thermal stress [22]. To ascertain the effect of thermal sensitive regions discussed above, we excluded them fictitiously from the calculation and illustrated the results in Fig. 6C (1UGQ) and Fig. 6D (1V29), respectively. For 1UGQ, the exclusion involved the hyper-sensitive regions of A1, A2, N-α-terminal and C-α-terminal, totally 713 atoms. After the exclusion, the average radius decreased to 21.7 Å below 350 K, and the expanding rate was also significantly reduced at 370 K (Fig. 6C). Apparently, these excluded regions answer for the expanding and denaturizing

Table 2
Salt-bridge interactions involving main chain atoms in region A1 of 1V29.

Amino acids		Occupied time (%)	Distance (Å)	Angle (°)
300 K				
ASP$^{204\text{-}O1}$	GLU^{241}*	100	3.101	25.07
ASP$^{204\text{-}O2}$	GLU^{241}*	95	4.280	48.06
GLU$^{241\text{-}O1}$	ARG^{203}*	93	3.536	19.06
GLU$^{241\text{-}O2}$	ARG^{203}*	89	3.821	18.81
320 K				
GLU$^{241\text{-}O2}$	ARG^{203}*	96	3.650	21.44
ASP$^{204\text{-}O1}$	GLU^{241}*	87	3.633	34.05
ASP$^{204\text{-}O2}$	GLU^{241}*	82	4.200	42.77
GLU$^{241\text{-}O1}$	ARG^{203}*	79	3.122	29.04
350 K				
ASP$^{204\text{-}O2}$	GLU^{241}*	90	3.572	28.89
GLU$^{241\text{-}O1}$	ARG^{203}*	89	3.695	22.18
ASP$^{204\text{-}O1}$	GLU^{241}*	79	4.014	43.82
GLU$^{241\text{-}O2}$	ARG^{203}*	59	3.196	29.27
370 K				
GLU$^{241\text{-}O1}$	ARG^{203}*	68	3.733	23.31
GLU$^{241\text{-}O2}$	ARG^{203}*	61	3.729	23.53

Note: The asterisk means that the hydrogen bonding acceptor is a main-chain atom. Time occupancy cutoff during the simulation is 50%. Distance cutoff is 5.00 angstroms (Å), and O–H–N angle cutoff is 120.00°. Intra-residue interactions were not included. Data were sorted by the value of the occupied time.

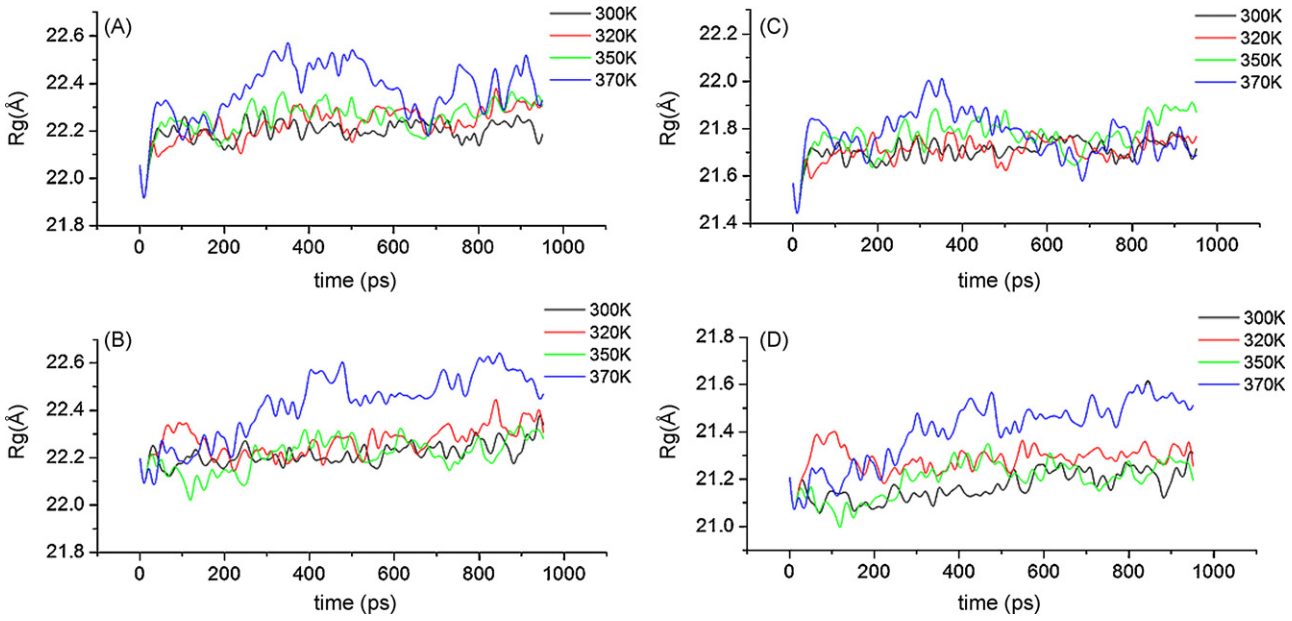

Fig. 6. Radius of gyration (R_g) profiles of 1UGQ and 1V29 containing or eliminating thermal sensitive regions at enhancing temperatures of 300 K (black), 320 K (red), 350 K (green) and 370 K (blue). (A) R_g calculated by the intact structure of 1UGQ. (B) R_g calculated by the intact structure of 1V29. (C) R_g calculated by the part structure of 1UGQ with exclusion of A1, A2, and N-, C-terminals of the α-subunit. (D) R_g calculated by the part structure of 1V29 with exclusion of regions B1 and N-, C-terminals of both α-subunit and β-subunit.

process of 1UGQ. For 1V29, region B1 and all terminals of both α- and β-subunit, totally 606 atoms were excluded. The average radius decreased to 21.2 Å below 350 K, indicating that the hydrophobic core of 1V29 exhibits a higher compactness than 1UGQ. The expanding rate had no significant reduction (Fig. 6D), indicating that the excluded regions in 1V29 were less sensitive to thermal stress than those in 1UGQ.

3.7. Strategy to improve thermal stability of the mesophilic NHase

Collectively, we would say that thermal sensitive regions differentiated by high RMSFs as discussed above should be responsible for the initial heat denaturation. Stabilizing these regions would be effective to improve the global thermal stability of the NHase. However, it is certainly impossible to directly delete these thermal sensitive regions from NHases as the imaginary calculations in Fig. 6. But we can elicit some constructive modification strategies from the MD simulation to improve the thermal stability of those industrialized mesophilic NHases.

Specify one industrialized mesophilic NHase, AY168347, as the target and compare its protein sequence with 1UGQ and 1V29. We found that its full-length identity is 42.7% and 40.2% with 1UGQ and 1V29, respectively. But for those corresponding thermal sensitive regions A1, A2, B1 and C-β-terminal in the mesophilic AY168347, we found much more non-conserved sequence in comparison to the thermophilic 1UGQ and 1V29 (Fig. 3).

Detailed sequence alignment in Fig. 3 revealed that it should be feasible to introduce the hook–hook like structure in region A1 of 1V29 into the mesophilic NHase of AY168347 by importing the 223-KEE-225 mutations in combination with the 228P/T-mutation. It is also feasible to introduce the stable salt-bridges in region A2 of 1V29 and C-β-terminal of 1UGQ into AY168347. Preliminary experimental mutations in region A1 of AY168347 have confirmed that mutations in this region significantly affected its thermal stability. More experiments directed by this MD simulation are in progress to improve the thermostability of the industrialized NHase.

4. Conclusions

Based on RMSF calculation of thermophilic NHases named 1UGQ and 1V29 at increasing temperature, several thermal sensitive regions were identified such as A1 and A2 in 1UGQ, B1 in 1V29, and most of the terminal ends in both enzymes. Comprehensive analyses of salt-bridge interactions within thermal stable and thermal sensitive regions showed that, in one hand, the formation of salt-bridges can significantly improve the thermal stability of enzymes; in the other hand, most of salt-bridges in the thermal sensitive regions are not strong enough to "spike" their adjacent structures from dissolving into solvent.

Considering the relatively high sequence similarity in all of the Co-type NHases [1], it's reasonable to suppose that the mesophilic NHases have similar heat denaturing mechanism with the thermophilic ones. Therefore, introducing one or more stable salt-bridges into thermal sensitive regions of the industrialized mesophilic NHases [23,24], as suggested by this simulation, would be promising to markedly increase their thermal stability.

Acknowledgements

This work is supported by the Foundation for the Author of National Excellent Doctoral Dissertation (No. 200345), the National High-tech Project 863 (2007AA02Z201) and the National Key Basic Research Project 973 (2007CB714304) of PR China.

References

[1] H. Yamada, M. Kobayashi, Nitrile hydratase and its application to industrial production of acrylamide, Biosci. Biotechnol. Biochem. 60 (1996) 1391–1400.
[2] I. Watanabe, Y. Satoh, K. Enomoto, Screening, isolation and taxonomical properties of microorganisms having acrylonitrile hydrating activity, Agric. Biol. Chem. 51 (1987) 3193–3199.
[3] T. Nagasawa, H. Nanba, K. Ryuno, K. Takeuchi, H. Yamada, Nitrile hydratase of *Pseudomonas chlororaphis* B23 purification and characterization, Eur. J. Biochem. 162 (1987) 691–698.
[4] T. Nagasawa, H. Shimizu, H. Yamada, The superiority of the third-generation catalyst, *Rhodococcus rhodochrous* J1 nitrile hydratase, for industrial production of acrylamide, Appl. Microbiol. Biotechnol. 40 (1993) 189–195.

[5] M. Lehmann, L. Pasamontes, S.F. Lassen, M. Wyss, The consensus concept for thermostability engineering of proteins, Biochim. Biophys. Acta 1543 (2000) 408–415.
[6] M. Karplus, Special issue on: molecular dynamics simulation on biomolecules, Acc. Chem. Res. 35 (2002) 321–323.
[7] A. Grottesi, M.A. Ceruso, et al., Molecular dynamics study of a hyperthermophilic and a mesophilic rubredoxin, Proteins: Struct. Funct. Genet. 40 (2002) 287–294.
[8] A.D. Gruia, S. Fischer, J.C. Smith, Molecular dynamics simulation reveals a surface salt bridge forming a kinetic trap in unfolding of truncated *Staphylococcal* nuclease, Proteins: Struct. Funct. Genet. 50E (2003) 507–515.
[9] J. Yin, D. Bowen, W.M. Southerland, Barnase thermal titration via molecular dynamics simulations: detection of early denaturation sites, J. Mol. Graph. Mod. 24 (2006) 233–243.
[10] E. Bae, G.N. Phillips Jr., Identifying and engineering ion pairs in adenylate kinases, J. Biol. Chem. 280 (2005) 30943–30948.
[11] A. Miyanaga, S. Fushinobu, K. Ito, H. Shoun, T. Wakagi, Mutational and structural analysis of cobalt-containing nitrile hydratase on substrate and metal binding, Eur. J. Biochem. 271 (2004) 429–438.
[12] A. Miyanaga, S. Fushinobu, K. Ito, T. Wakagi, Crystal structure of cobalt-containing nitrile hydratase, Biochem. Biophys. Res. Commun. 288 (2001) 1169–1174.
[13] S. Hourai, M. Miki, et al., Crystal structure of nitrile hydratase from a thermophilic *Bacillus smithii*, Biochem. Biophys. Res. Commun. 312 (2003) 340–345.
[14] R. Pereira, D. Graham, F. Rainey, D. Cowan, A novel thermostable nitrile hydratase, Extremophiles 2 (1998) 347–357.
[15] D.A. Case, T.A. Darden, T.E. Cheatham III, C.L. Simmerling, J. Wang, R.E. Duke, R. Luo, K.M. Merz, B. Wang, D.A. Pearlman, M. Crowley, S. Brozell, V. Tsui, H. Gohlke, J. Mongan, V. Hornak, G. Cui, P. Beroza, C. Schafmeister, J.W. Caldwell, W.S. Ross, P.A. Kollman, AMBER 8, University of California, San Francisco, 2004.
[16] J. Wang, P. Cieplak, P.A. Kollman, How well does a restrained electrostatic potential (RESP) model perform in calculating conformational energies of organic and biological molecules, J. Comput. Chem. 21 (2000) 1049–1074.
[17] C.L. Brooks, M. Karplus, B.M. Pettitt, Proteins: A Theoretical Perspective of Dynamics, Structure, and Thermodynamics: Advances in Chemical Physics LXXI, John Wiley & Sons, New York, 1988.
[18] W. Humphrey, A. Dalke, K. Schulten, VMD—visual molecular dynamics, J. Mol. Graph. Mod. 14 (1996) 33–38.
[19] D.A. Cowan, R.A. Cameron, T.L. Tsekoa, Comparative biology of mesophilic and thermophilic nitrile hydratases, Adv. Appl. Microb. 52 (2003) 123–153.
[20] E.E. Bastawissy, M.H. Knaggs, I.H. Gilbert, Molecular dynamics simulations of wild-type and point mutation human prion protein at normal and elevated temperature, J. Mol. Graph. Mod. 20 (2001) 145–154.
[21] M. Feig, J. Karanicolas, C.L. Brooks, III: MMTSB Tool Set, MMTSB NIH Research Resource, The Scripps Research Institute, 2001.
[22] C. Scharnagl, M. Reif, J. Friedrich, Stability of proteins: temperature, pressure and the role of the solvent, Biochim. Biophys. Acta 1749 (2005) 187–213.
[23] Y. Shi, H.M. Yu, X.D. Sun, Z.L. Tian, Z.Y. Shen, Cloning of the nitrile hydratase gene from *Nocardia* sp. in *Escherichia coli* and *Pichia pastoris* and its functional expression using site-directed mutagenesis, Enz. Microb. Technol. 35 (2004) 557–562.
[24] H.M. Yu, Y. Shi, H. Luo, Z.L. Tian, Y.Q. Zhu, Z.Y. Shen, An over expression and high efficient mutation system of a cobalt-containing nitrile hydratase, J. Mol. Catal. B: Enz. 43 (2006) 80–85.